

Gravitational binding in 4D dynamical triangulation

Bas V. de Bakker*

Centre for High Energy Astrophysics
Kruislaan 403, 1098 SJ Amsterdam, the Netherlands.

Jan Smit[‡]

Institute for Theoretical Physics, University of Amsterdam
Valckenierstraat 65, 1018 XE Amsterdam, the Netherlands.

April 26, 1996

Abstract

In the dynamical triangulation model of four dimensional euclidean quantum gravity we investigate gravitational binding. Two scalar test particles (quenched approximation) have a positive binding energy, thereby showing that the model can represent gravitational attraction.

*email: bas@astro.uva.nl

‡email: jsmit@phys.uva.nl

1 Introduction

The dynamical triangulation model has been proposed as a purely discrete regularisation of euclidean quantum gravity [1, 2] (for a similar earlier proposal see [3]). As a model of gravity it ought to have a scaling regime where it corresponds to semiclassical Einstein gravity. One wishes to recover classical euclidean spacetimes, Newton's potential and the formation of gravitationally bound states.

It is not clear that a purely euclidean formulation should be able to contain semiclassical gravity, because of the well known divergence related to the unboundedness of the euclidean version of the Einstein-Hilbert action. In a semiclassical evaluation of the euclidean path integral this can be dealt with by deforming the integration over the conformal mode into the imaginary direction of the complex plane [4].

The dynamical triangulation formulation is completely regular from the start. The model has a phase transition as a function of a parameter which is proportional to the inverse bare Newton constant: $\kappa_2 \propto G_0^{-1}$. The transition separates a phase with crumpled spacetimes and very high effective dimensionalities, from an 'elongated' phase with effectively two-dimensional spacetimes with characteristics of a branched polymer [5, 6]. Near the transition the model appears to produce classical S^4 -like spacetimes, in an intermediate distance regime, and there is evidence for scaling, suggesting continuum behaviour [5, 7]. In the elongated phase the scaling degenerates into a branched polymer version [6]. The scaling appears compatible with recent evidence that the transition is of first order [7, 8], instead of second order as thought previously. The first order nature of the transition need of course not stand in the way of continuum behaviour, as the examples of gauge-Higgs models show.

It is of great interest to find out if this scaling region can be described by an effective action of the type

$$S_{\text{eff}} = \int d^4x \sqrt{g} \left(\frac{\Lambda}{8\pi G} - \frac{R}{16\pi G} + \alpha R^2 + \dots \right). \quad (1)$$

The branched polymer phase is presumably an expression of the conformal mode instability of the $-R/G$ -part in this effective action at scales of order \sqrt{G} , while the crumpled phase may correspond to negative G . Such an interpretation deserves separate elaboration, which falls outside the scope of this paper.

It would be very interesting if we could measure the attraction of two sources at a fixed distance. This has been attempted in the Regge calculus formulation of simplicial quantum gravity [9], although with sources at a fixed distance with respect to the triangulation, i.e. to a background metric instead of to the fluctuating metric. Such measurements could then be compared with the simple Newtonian law or with quantum corrections to this law, which have for instance been calculated in [10] and [11]. In dynamical triangulation a computation of the gravitational potential appears nontrivial, because it is difficult in a fluctuating spacetime to keep two heavy test masses at a fixed distance.

However, the formation of bound states out of two test particles can be computed in a way that is customary in lattice field theory and we shall report on such computations in this paper. A preliminary account of this has appeared already in [12] and [13].

2 Binding in the continuum

Consider a free scalar field ϕ with bare mass m_0 in a quantum gravity background. In continuum language, the euclidean action of this system is a sum of a gravitational and a matter part

$$S = S[g] + S[g, \phi], \quad (2)$$

$$S[g] = \frac{1}{16\pi G_0} \int d^4x \sqrt{g} (2\Lambda_0 - R), \quad (3)$$

$$S[g, \phi] = \int d^4x \sqrt{g} \left(\frac{1}{2} g^{\mu\nu} \partial_\mu \phi \partial_\nu \phi + \frac{1}{2} m_0^2 \phi^2 \right), \quad (4)$$

where Λ_0 is the bare cosmological constant, R is the scalar curvature and G_0 is the bare Newton constant.

We take ϕ as a test particle here, i.e. the back reaction of the field ϕ on the metric is not taken into account. In lattice QCD this approximation is often called the quenched approximation, or valence quark approximation, because it neglects diagrams with internal quark (in our case ϕ) loops. For not too light quark masses it turns out to give good results (for a discussion see e.g. [14]). In dynamical triangulation the inclusion of a scalar field is no problem in principle (and appears to have little influence on the gravity sector of the theory) [15], but the enlargement of parameter space by m_0

is computationally costly. A continuum calculation of the gravitational attraction of a scalar field in the quenched approximation was carried out in [10].

We will use the following notation for expectation values of an observable A . On a fixed background geometry we can average over configurations of the matter field

$$\langle A \rangle_\phi = \frac{\int \mathcal{D}\phi A \exp(-S[g, \phi])}{\int \mathcal{D}\phi \exp(-S[g, \phi])}, \quad (5)$$

and we can average over metrics

$$\langle A \rangle_g = \frac{\int \mathcal{D}g A \exp(-S[g])}{\int \mathcal{D}g \exp(-S[g])}, \quad (6)$$

The quenched expectation value is then

$$\langle A \rangle = \langle \langle A \rangle_\phi \rangle_g. \quad (7)$$

We next consider propagators in a fixed geometry. The one particle propagator, denoted by $G(x, y; g)$, is defined as

$$G(x, y; g) = \langle \phi_x \phi_y \rangle_\phi. \quad (8)$$

The connected two-particle propagator will then be the square of the one particle propagator

$$\langle \phi_x \phi_x \phi_y \phi_y \rangle_\phi^{\text{conn}} = G(x, y; g)^2. \quad (9)$$

Giving the two particles a different flavour quantum number this would be the complete two-particle propagator. The disconnected part is not immediately suitable for bound state calculations in the quenched approximation (as with the η' particle in quenched QCD).

Letting the metric fluctuate, we take the average of the propagators over the different metrics. Because of reparametrisation invariance, the average $\langle G(x, y; g) \rangle_g$ can only depend on whether x and y coincide or not. Therefore, we look at averages at fixed geodesic distance r ,

$$G(r) = \left\langle \frac{\int d^4x \sqrt{g} G(x, y; g) \delta(d(x, y) - r)}{\int d^4x \sqrt{g} \delta(d(x, y) - r)} \right\rangle_g, \quad (10)$$

where $d(x, y)$ is the minimal geodesic distance between x and y . By translation invariance, the resulting $G(r)$ is independent of y . Similarly, we can define the geometry average of the two-particle propagator as

$$G^{(2)}(r) = \left\langle \frac{\int d^4x \sqrt{g} G(x, y; g)^2 \delta(d(x, y) - r)}{\int d^4x \sqrt{g} \delta(d(x, y) - r)} \right\rangle_g. \quad (11)$$

In (10) we first averaged over the volume at distance r from the point y and then averaged over the metrics. Alternatively we can integrate $G(x, y; g)$ over the volume at distance r , average over metrics, and then divide by the same with $G \rightarrow 1$,

$$G(r) = \frac{\left\langle \int d^4x \sqrt{g} G(x, y; g) \delta(d(x, y) - r) \right\rangle_g}{\left\langle \int d^4x \sqrt{g} \delta(d(x, y) - r) \right\rangle_g}. \quad (12)$$

A similar ambiguity arises with purely geometric correlators [16]. Our physical intuition tends to favour the form (10), and we shall later use its analogue in dynamical triangulation. However, if there is no pair x, y with $d(x, y) = r$ for a given metric g the expression becomes mathematically ill defined, whereas (12) has no such problem. For the pure geometry correlators this does not happen in practise for reasonable r and the difference between (10) and (12) appears to be small [17].

For a massive particle, we expect the propagator (10) to fall off exponentially as

$$G(r) \propto r^\alpha \exp(-mr), \quad (13)$$

with some power α and renormalised mass m , which in general will not equal the bare mass m_0 . This expression neglects finite size effects and should be modified when looking at distances comparable to a typical length scale in the system.

The two-particle propagator will behave similarly as

$$G^{(2)}(r) \propto r^\beta \exp(-Mr), \quad (14)$$

where M is the energy of the two-particle state. If this energy turns out to be less than two times the mass of a single particle, the difference can be interpreted as a binding energy between the particles. This would show gravitational attraction between them.

3 Propagating in constant curvature

Since the spacetimes to be used in the binding energy computations have topology S^4 and the average spacetime is expected to be homogeneous, it will be useful to know the properties of scalar field propagators on spaces of constant curvature. To calculate such propagators we have to solve the equation

$$(\square - m^2)G = 0, \quad (15)$$

with the boundary condition $G \rightarrow (4\pi^2 r^2)^{-1}$ as the geodesic distance $r \rightarrow 0$. We assume spherical symmetry, i.e. G depends only on r . We need to distinguish three cases: positive, zero and negative curvature. For a space with constant positive curvature, i.e. a four-sphere, equation (15) can be written as

$$(\partial_x + 3 \cot x)\partial_x G - m^2 r_0^2 G = 0, \quad (16)$$

where $x = r/r_0$, with r_0 the curvature radius. The substitution $z = \cos^2(x/2)$, which was used in [18], turns this into a hypergeometric equation,

$$[z(1-z)\partial_z^2 + (2-4z)\partial_z - m^2 r_0^2] G(z) = 0. \quad (17)$$

For numerical evaluation we found it easiest to use a series representation

$$G(z) = N \sum_{k=0}^{\infty} c_k z^k. \quad (18)$$

Setting $c_0 = 1$, the differential equation fixes the c_k as

$$c_k = \frac{(k+2)(k-1) + m^2 r_0^2}{k(k+1)} c_{k-1}, \quad (19)$$

If we demand that the singularity at the origin goes like $(4\pi^2 r^2)^{-1}$, this fixes the normalisation to be

$$N = \frac{m^2 r_0^2 - 2}{16\pi r_0^2 \cosh\left(\pi \sqrt{m^2 r_0^2 - \frac{9}{4}}\right)}. \quad (20)$$

One can easily check that this function also conforms to the differential equation at the point opposite the origin, where $x = \pi$. When the mass is so small that $m^2 r_0^2 < 9/4$, the above formulas may be analytically continued such that

$$N = \frac{m^2 r_0^2 - 2}{16\pi r_0^2 \cos\left(\pi \sqrt{\frac{9}{4} - m^2 r_0^2}\right)}. \quad (21)$$

The negative curvature case gives similarly

$$(\partial_x + 3 \coth x) \partial_x G - m^2 r_0^2 G = 0. \quad (22)$$

Using the substitution $z = \operatorname{sech} x$, we get

$$[(1 - z^2)z^2 \partial_z^2 + (-2 - 2z^2)z \partial_z - m^2 r_0^2] G(z) = 0. \quad (23)$$

In this case we use the series

$$G(z) = N \sum_{k=0}^{\infty} c_k z^{k+\mu}, \quad (24)$$

and the recurrence equation is now

$$c_k = \frac{(k + \mu - 2)(k + \mu - 1)}{(k + \mu)(k + \mu - 3) - m^2 r_0^2} c_{k-2}. \quad (25)$$

We can read off that we have to choose

$$\mu = \frac{3}{2} + \sqrt{\frac{9}{4} + m^2 r_0^2}, \quad (26)$$

to avoid generating negative powers of z . Setting again $c_0 = 1$ and demanding that G goes like $(4\pi^2 r^2)^{-1}$ for small r gives us the normalisation

$$N = \frac{\Gamma(\mu/2)\Gamma(\mu/2 + 1/2)}{4\pi^2 r_0^2 \Gamma(\mu - 1/2)}. \quad (27)$$

The flat case is the easiest. Using the spherical symmetry results in

$$\left(\partial_r + \frac{3}{r}\right) \partial_r G(r) - m^2 G(r) = 0, \quad (28)$$

which can be directly solved in terms of a Bessel function as

$$G(r) = \frac{m K_1(mr)}{4\pi^2 r}, \quad (29)$$

using the condition that $G(r)$ goes like $(4\pi^2 r^2)^{-1}$ for small r .

We have plotted an example of the three cases in figure 1, using a curvature radius r_0 of 13 and a mass m of 0.15. These parameters were chosen for later comparison with dynamical triangulation results.

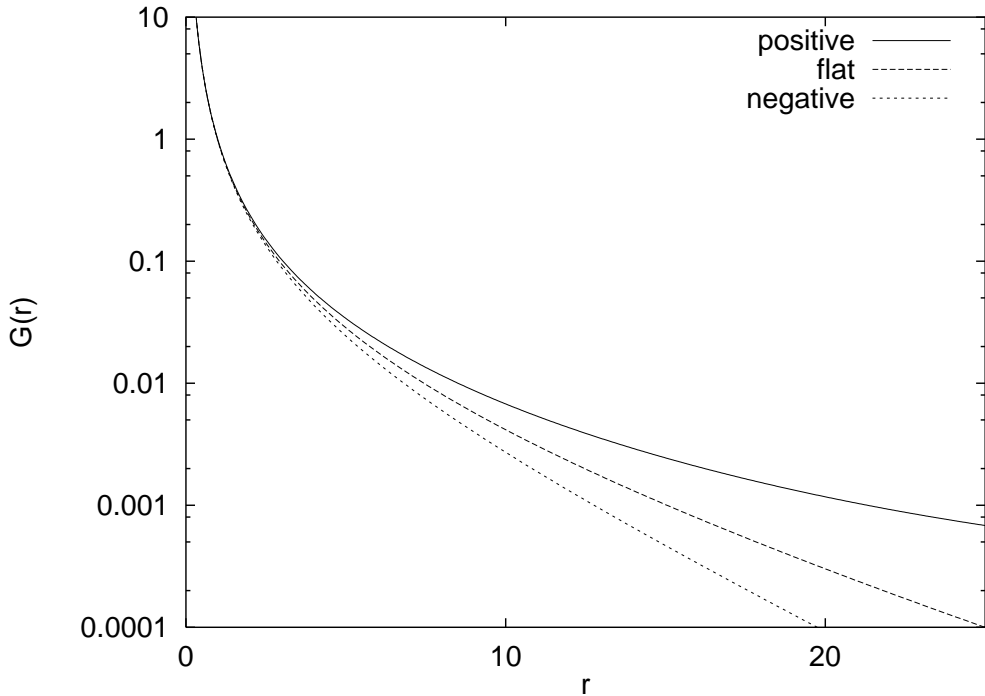


Figure 1: Propagators on spaces with constant curvature $R = 12/r_0^2$ (upper), $R = 0$ (middle) and $R = -12/r_0^2$ (lower), with $r_0 = 13$ and $m = 0.15$.

4 Dynamical triangulation

In the dynamical triangulation model of four dimensional euclidean quantum gravity the path integral over metrics on a certain manifold is defined by a weighted sum over all ways to glue four-simplices together at the faces [1, 2]. This idea was first formulated in [3], using hypercubes instead of simplices. In four dimensions the analogue of the continuum gravitational action is

$$S[g] = \frac{1}{16\pi G_0} \int d^4x \sqrt{g} (2\Lambda_0 - R) \quad (30)$$

$$\rightarrow \kappa_4 N_4 - \kappa_2 N_2, \quad (31)$$

where N_2 and N_4 are the number of triangles and four-simplices respectively.

The partition function of the model for a fixed volume (fixed number of

four-simplices N_4) is given by

$$Z(N, \kappa_2) = \sum_{\mathcal{T}(N_4=N)} \exp(\kappa_2 N_2). \quad (32)$$

The sum is over all ways to glue N four-simplices together, such that the resulting complex satisfies the manifold condition, with some fixed topology which is usually (as well as in this article) taken to be S^4 . The coupling constant κ_2 is proportional to the inverse of the bare Newton constant:

$$\kappa_2 = V_2/4G_0, \quad (33)$$

where V_2 is the area of a triangle.

It turns out that the model has two phases [19, 20, 21, 22]. For low κ_2 the system is in a crumpled phase, where the average number of simplices around a vertex is large and the average distance between two simplices is small. In this phase the volume within a distance r appears to increase exponentially with r , a behaviour like that of a space with constant negative curvature. At high κ_2 the system is in an elongated phase and resembles a branched polymer. As is the case with a branched polymer, the (large scale) internal fractal dimension is 2. The transition between the two phases occurs at a critical value κ_2^c which depends somewhat on N . The phase transition appears to be of first order [7, 8]. At the transition (on the crumpled side) the spaces behave on the average in several respects like the four dimensional sphere [5]. Some of the evidence for this will be reviewed in the next section.

5 Spacetimes near the transition

We have performed numerical simulations of four dimensional dynamical triangulation, according to the partition function (32). We used systems of about 32000 simplices and the topology of the four-sphere. To keep the number of simplices around the desired value, we added a quadratic term to the action as was described in [19, 22, 23].

In ref. [5] we studied the euclidean spacetimes generated in numerical simulations of the model by measuring the number of simplices $N'(r)$ at geodesic distance r . (The geodesic distance d_{xy} between two simplices with centres x and y is defined as the minimum number of links on the dual lattice between x and y .) We fitted $N'(r)$ in an intermediate distance regime by a

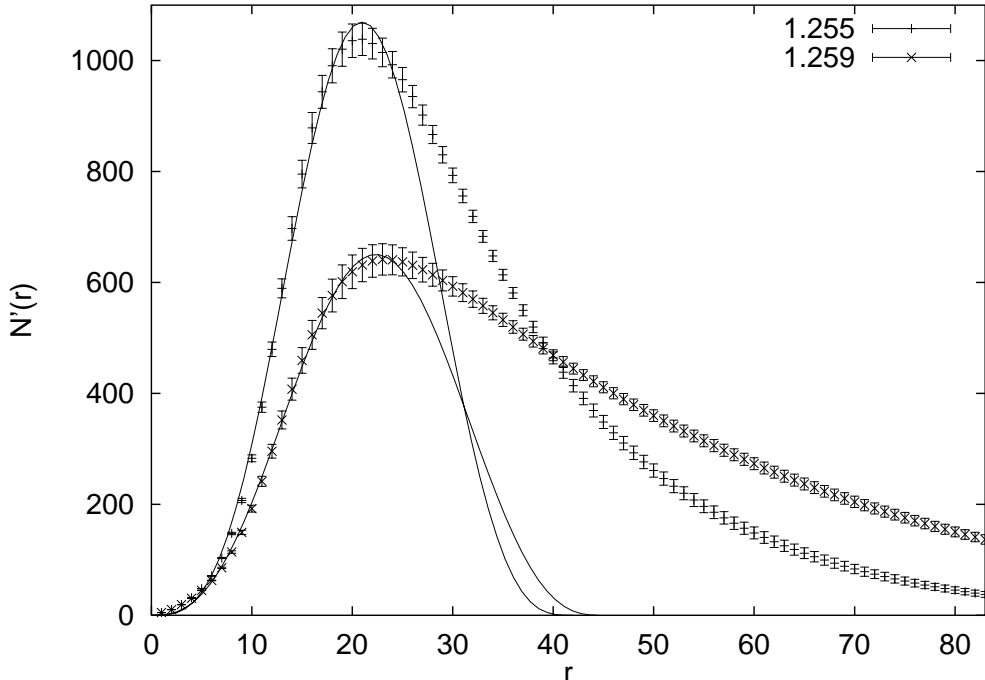


Figure 2: Fits to $N'(r)$ of the form $a \sin^{d-1}(r/r_0)$ near the transition. Upper curve: $\kappa_2 = 1.255$, $d = 4.24(4)$, $r_0 = 13.35(7)$; lower curve: $\kappa_2 = 1.259$, $d = 3.67(7)$, $r_0 = 14.2(2)$.

form $c \sin^{d-1}(r/r_0)$ corresponding to a d -sphere of radius r_0 . For κ_2 near the transition $\kappa_2^c(N)$ this gave $d \approx 4$, which we took as evidence for classical S^4 behaviour at the distance scale involved. Below the transition (i.e. $\kappa_2 < \kappa_2^c$) d rises steeply to large values while above the transition d falls rapidly to the branched polymer value $d = 2$.

To get a feeling for the geodesic distances which will appear later in binding energy computations, we show in fig. 2 the quantity $N'(r)$ for a system of $N = 32000$ simplices at $\kappa_2 = 1.255$ and 1.259 . The value 1.255 is very near $\kappa_2^c(N)$ as defined by the position of the maximum in the susceptibility

$$\frac{\partial^2 \ln Z(N, \kappa_2)}{N \partial \kappa_2^2} \approx N \left[\left\langle \frac{N_2^2}{N_4^2} \right\rangle - \left\langle \frac{N_2}{N_4} \right\rangle^2 \right]. \quad (34)$$

The $\sin^{d-1}(r/r_0)$ -fit gives $d = 4.24(4)$ and is seen to be reasonable in the

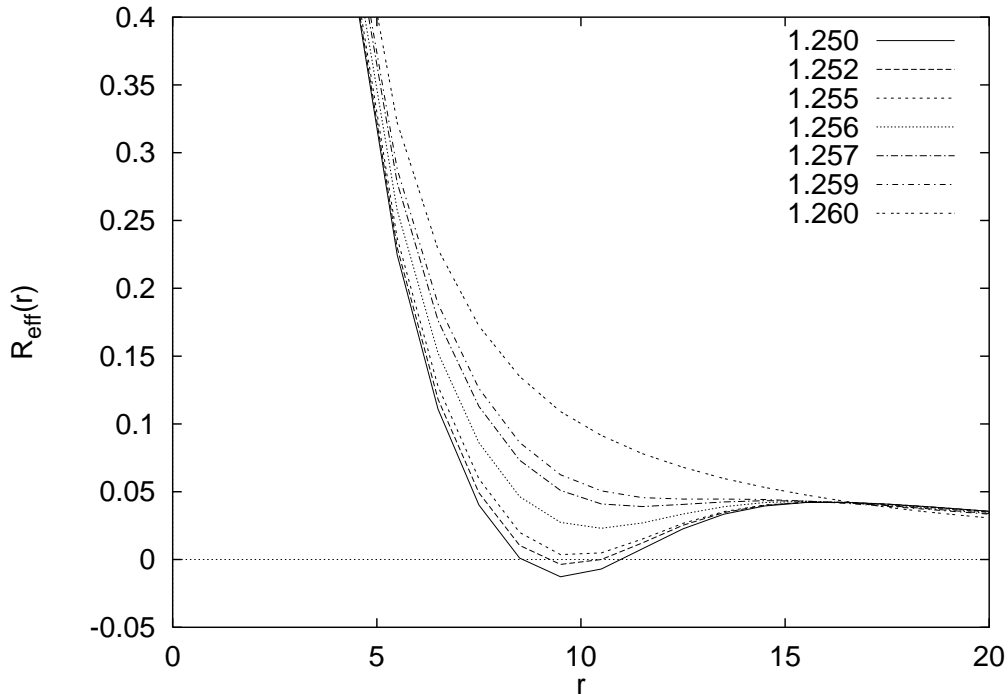


Figure 3: Effective curvature plots for $\kappa_2 = 1.250$ – 1.260 .

region $6 \leq r \leq 24$. The value 1.259 is our κ_2 closest to the phase transition for which the data fit the four-sphere also reasonably well with $d = 3.67(7)$, in the region $5 \leq r \leq 25$. The overall shape of $N'(r)$ is quite asymmetrical, which is presumably due to branching fluctuations at larger distances.

In [5] we also introduced an effective curvature $R_{\text{eff}}(r)$ to describe the curvature at scales much larger than the lattice scale. The argument r of $R_{\text{eff}}(r)$ is meant to approach zero provided that, and as long as, $R_{\text{eff}}(r)$ is stationary. This does not seem to happen in the elongated phase, while near the transition and in the crumpled phase we found that R_{eff} had indeed a stationary point (minimum). For smaller r -values R_{eff} rises steeply when r gets smaller. We called this region of large R_{eff} the ‘planckian regime’.

Fig. 3 shows R_{eff} for $N = 32000$ and several values of κ_2 . For $\kappa_2 < 1.255$ we see negative curvature at the minimum of R_{eff} . A homogeneous space with constant negative curvature is unbounded, so the maximum in $N'(r)$ is evidently due to finite size effects. We take the ‘planckian regime’ as the small r region, roughly ending at the minimum of R_{eff} . For $\kappa_2 = 1.255$ the

effective curvature is nearly zero at the minimum, while positive for larger κ_2 . The minimum has roughly turned into an inflection point at $\kappa_2 = 1.259$, and it has disappeared altogether for larger κ_2 .

Fig. 2 suggests positive curvature with a curvature radius of $r_0 \approx 21/(\pi/2) \approx 13$. This corresponds to some average near the minima in fig. 3. The minima will show somewhat smaller curvature: $R_{\text{eff}}(r_{\text{min}}) \approx 0, 0.045$, for $\kappa_2 = 1.255, 1.259$, respectively. The latter minimum corresponds to a curvature radius $r_0 = \sqrt{12/0.045} \approx 16$, which is not unreasonable compared to the previous 13.

We conclude that for $\kappa_2 = 1.255 - 1.259$ the spacetimes are on the average near S^4 in the distance regime $6 \leq r \leq 24$.

6 Binding in dynamical triangulation

On each dynamical triangulation configuration we calculated the propagator of the scalar field

$$G_{xy} = (-\square + m_0^2)_{xy}^{-1}, \quad (35)$$

using the algebraic multigrid routine AMG1R5, where x is an arbitrary origin. The discrete Laplacian is defined as

$$(\square)_{xy} = \begin{cases} 1 & \text{if } x \text{ and } y \text{ are nearest neighbours,} \\ -5 & \text{if } x = y, \\ 0 & \text{otherwise.} \end{cases} \quad (36)$$

The 5 in the second line arises as the coordination number of a four-simplex, i.e. a four-simplex has five neighbours.

We can then calculate $G(r)$ and $G^{(2)}(r)$ by averaging G_{xy} respectively its square over all points y at distance r from the origin x , and then over origins and configurations,

$$G(r) = \left\langle \frac{\sum_y G_{xy} \delta_{d_{xy}, r}}{\sum_y \delta_{d_{xy}, r}} \right\rangle_g, \quad (37)$$

$$G^{(2)}(r) = \left\langle \frac{\sum_y G_{xy}^2 \delta_{d_{xy}, r}}{\sum_y \delta_{d_{xy}, r}} \right\rangle_g \quad (38)$$

(we have not indicated the average over origins x). Notice that (37) corresponds to (10) in the continuum.

To improve the calculation of the binding energy, we can try to use what are called “smeared sources”. The use of these smeared sources can improve the data by increasing the contribution of the ground state and decreasing the contribution of the excited states. Instead of using (38), we can calculate $G(r)$ by averaging G_{xy} over all points at distance r from the origin x , and only after taking this average, square it for the calculation of $G^{(2)}(r)$:

$$G^{(2)}(r) = \left\langle \left(\frac{\sum_y G_{xy} \delta_{d_{xy},r}}{\sum_y \delta_{d_{xy},r}} \right)^2 \right\rangle_g. \quad (39)$$

This corresponds to taking the propagator from a source that is not a single point, but a complete shell around the origin. Such a source may have a bigger overlap with the ground state wave function and a smaller one with the excited wave functions. For a discussion of the use of these smeared sources in QCD, see e.g. [24].

Because the average of the square of a fluctuating quantity is always greater than the square of its average, it is obvious that $G^{(2)}(r) > G(r)$. This does not yet imply anything about the way they fall off. In particular it is not guaranteed that the energy of the two-particle state is less than twice the energy of the one particle states.

In figure 4 we see the results for four different bare masses. Each pair of lines corresponds to one bare mass. In each pair the upper line is $G^{(2)}(r)$ (using (38)) and the lower line is $G(r)^2$ of eq. (37). We used 144 configurations recorded every 5000 sweeps (1 sweep = N accepted moves). For each of the masses we used 120 origins per configuration. The coupling constant $\kappa_2 = 1.255$, which is the lower of the two κ_2 values used in the $N'(r)$ figure 2.

There is clearly a difference in slope between the lines in each pair. This shows that the energy of the two particle state is less than two times the mass of a single particle and consequently that there is a positive binding energy between the particles.

Using this data we can measure the renormalised mass m , by assuming a long distance behaviour of $r^\alpha \exp(-mr)$. The results are (in parenthesis is the value of κ_2)

m_0	$m(1.255)$	$m(1.259)$	m/m_0
0.0316	0.14	0.12	≈ 4.1
0.1	0.29	0.27	≈ 2.8
0.316	0.60	0.58	≈ 1.9
1	1.21	1.20	≈ 1.20

(40)

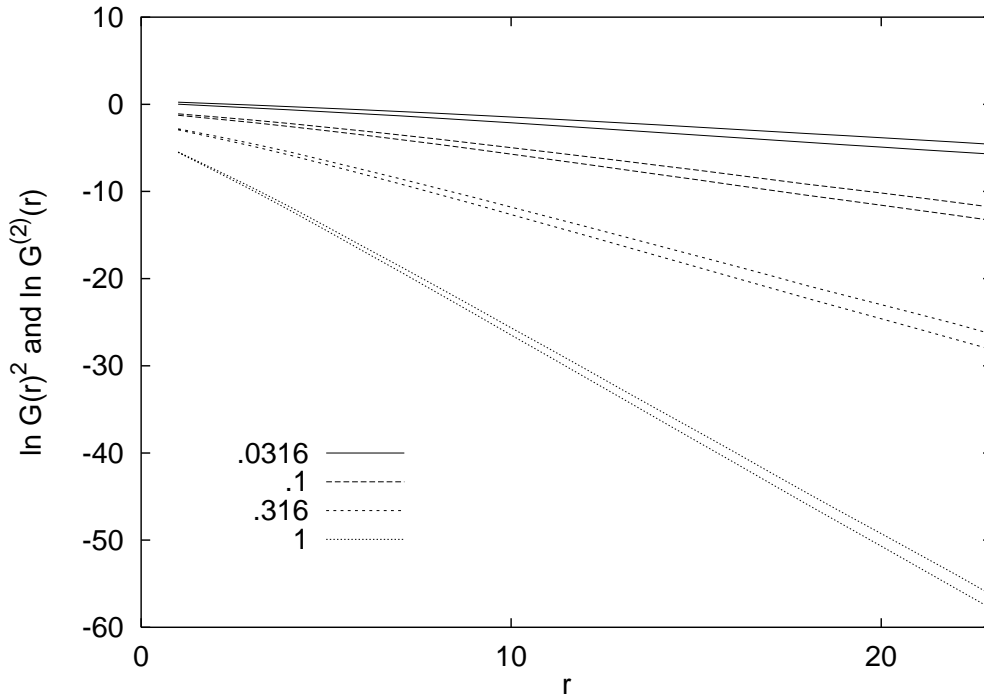


Figure 4: The two-particle propagator and the square of the one particle propagator versus the geodesic distance for four different bare masses m_0 . The vertical scale is logarithmic. $\kappa_2 = 1.255$, which is very close to the transition.

It was argued in [19] that the physical mass should vanish at zero bare mass and that therefore the renormalisation would be only multiplicative. Our data seem to show that the relation is more complicated. Increasing m_0 by a factor of $\sqrt{10} \approx 3.16$ increases m by a factor of about 2.1.

Comparing figure 1 with figure 4, we see that the long distance behaviour is indeed similar, being an exponential. The finite size effect of the S^4 -like curvature is apparently negligible, except perhaps for the smallest mass. The short distance behaviour is quite different. The propagators in figure 4 curve downward towards the origin, while the free propagators shown in figure 4 curve upwards due to the $1/r^2$ behaviour. The curving downward is unusual, because a propagator is interpreted as a sum of decaying exponentials corresponding to the ground state and various excited states. A closer look shows that the downward curvature occurs for distances smaller than about $r = 5$,

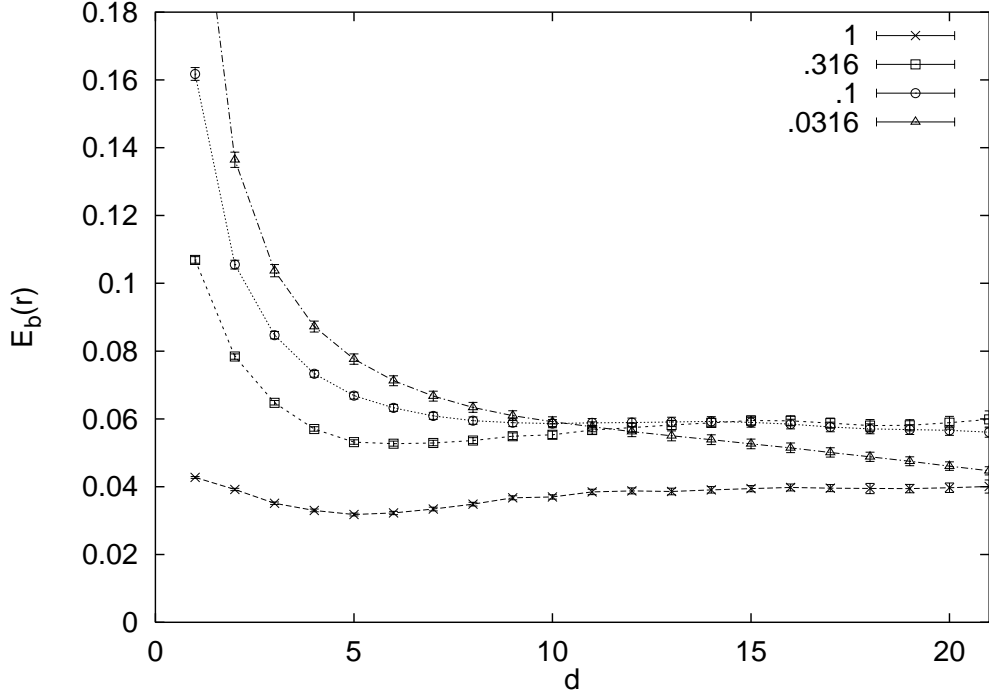


Figure 5: The effective binding energy E_b as a function of the geodesic distance for four different bare masses at $\kappa_2 = 1.255$.

which is roughly the end of the ‘planckian regime’ mentioned in the previous section. As we have seen in figure 1, larger positive curvature means that the propagator decreases more slowly. Therefore, such a planckian regime may cause the propagator to decrease less at smaller distances where the effective curvature is large than at the longer distances where the effective curvature is small.

Using these data, we can now estimate the binding energy of the particles. From (13) and (14) we have

$$E_b(r) \equiv r^{-1} \ln \frac{G^{(2)}(r)}{G(r)^2} \quad (41)$$

$$\rightarrow E_b = 2m - M, \quad r \rightarrow \infty. \quad (42)$$

As we cannot use infinite distances, we will consider the effective binding energy $E_b(r)$ for finite r and look whether this expression becomes constant.

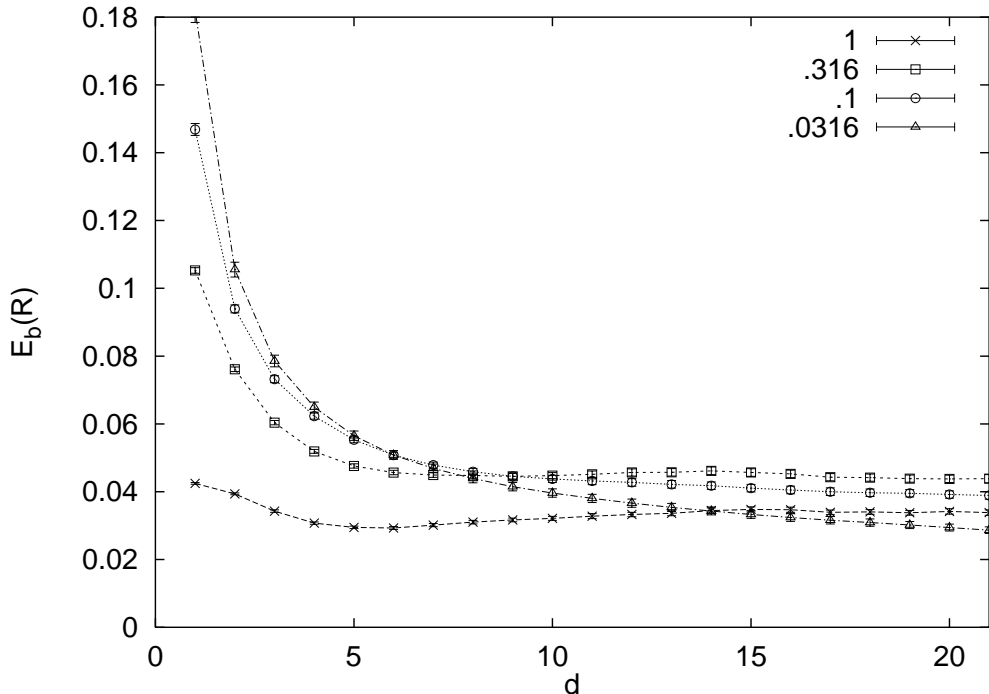


Figure 6: Like figure 5, but with $\kappa_2 = 1.259$.

Figure 5 shows this quantity as a function of the geodesic distance, using the smeared estimator (39) for $G^{(2)}(r)$. The four curves again correspond to the four different bare masses in figure 4. To avoid the correlations between origins on the same configuration and between points at the same distance of such an origin influencing the error bars, we first averaged all the measurements of each configuration and used a jackknife method on these averages to calculate the error bars.

It is clear that the binding energy goes to a non-zero value, with the exception of the lowest mass, where the effective binding energy does not seem to converge within the limited distance range. We chose not to display distances larger than the position of the maximum of $N'(r)$ in figure 2.

Unfortunately, the correlation between the mass and the binding energy does not appear to be strictly positive. The lowest binding energy belongs to the highest mass. We defer a more elaborate discussion to the next section.

Figure 6 shows the corresponding data for $\kappa_2 = 1.259$ which is the higher of the two κ_2 values used in figure 2 for $N'(r)$. In this case we used 200

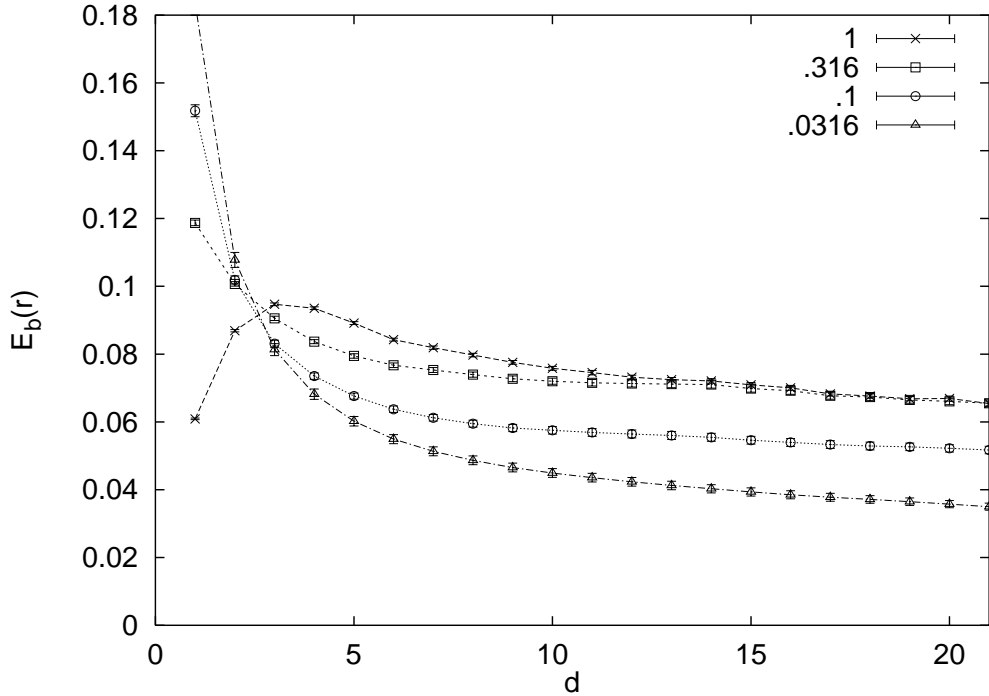


Figure 7: Like figure 6, but with unsmeared sources.

configurations, again with 120 origins per configuration. The data look very similar. Here the ordering of binding energies follows more clearly that of the constituent masses, except for the largest mass $m_0 = 1$.

To see the effect of using smeared sources we show in figure 7 the effective binding energy using the unsmeared estimator (38) for $\kappa_2 = 1.259$, the analogue of figure 6. The use of smeared sources (figure 6 compared to figure 7) does indeed improve the convergence to a definite value and the effective binding energies are generally smaller. In particular the curve for a bare mass of 1, which keeps going down in figure 5 becomes more horizontal. Only the smallest mass is an exception, where neither case has converged yet in the distance range shown.

7 Discussion

Despite the unboundedness of the Einstein-Hilbert part of the the euclidean effective action (1), the spacetimes produced by the dynamical triangulation model have semiclassical features near the phase transition, at least on the crumpled side. For the binding energy computations we have chosen the bare coupling $\kappa_2 \propto 1/G_0$ such that the volume at distance r , $N'(r)$, behaves like that of a four-sphere, for not too large distances r outside a ‘planckian regime’. The data for a nonzero binding energy are quite convincing and encouraging.

We would like to be able to extract the renormalised Newton constant G from the data, for example according to the nonrelativistic formula

$$E_b \equiv 2m - M = \frac{1}{4}G^2m^5. \quad (43)$$

This formula is just the familiar energy $\alpha^2 m_{\text{red}}/2$ of the hydrogen atom in the ground state, but with the gravitational parameters substituted as $\alpha \rightarrow Gm^2$ and the reduced mass $m_{\text{red}} \rightarrow m/2$. Because the formula (43) is nonrelativistic it may not suffice to fit the data. To get a rudimentary feeling for corrections to (43) we consider the hamiltonian

$$H = 2\sqrt{m^2 + p^2} - Gm^2/r. \quad (44)$$

Replacing $p \rightarrow 1/r$ and minimising the energy leads to

$$E_b = 2m - 2m\sqrt{1 - G^2m^4/4}, \quad (45)$$

which suggests that $Gm^2 = 2$ has to be considered ‘large’.

Unfortunately, the data in figure 5 or 6 show no sign of the m^5 behaviour of (43), and neither is (45) of any help. Even the largest constituent mass $m \approx 1.2$, which is evidently so large in lattice units that only qualitative conclusions may be drawn from it, leads to a small binding energy. For the lighter constituent masses the binding energy is only modestly dependent on m .

Perhaps the behaviour of the lightest constituent mass hints at a possible interpretation. Its effective binding energy has not converged yet for the distances shown which is a hint that the binding energy itself is substantially smaller than all the others. We cannot pursue this because we do not trust

distances much beyond the maximum of $N'(r)$ since these run into its asymmetric tail. Yet, if we make the bold assumption that the nonrelativistic formula (43) starts making sense for this smallest constituent mass $m \approx 0.13$ (the mean for $\kappa_2 = 1.255$ and 1.259) and use $E_b \approx 0.03$, we get for the renormalised Planck length $\sqrt{G} \approx 7.5$. This is quite a reasonable value and it is furthermore similar to the (somewhat vague) distance scale the planckian regime ends. On the other hand, the size of a nonrelativistic bound state is of order of $1/m$, so if indeed $\sqrt{G} \approx 7.5$, we should perhaps not be surprised to find odd behaviour for bound state sizes of the order of the Planck length, or constituent masses greater than the Planck mass $1/\sqrt{G} \approx 0.13$.

Clearly, we are having a problem of separating scales: we would like $\sqrt{G} \ll m^{-1} \ll r_m$, where $r_m = r_0\pi/2$ is a measure of the size of our S^4 -‘universe’ (the distance where the volume $N'(r)$ is maximal). In our situation, at best, $\sqrt{G} \approx m^{-1}$ and $r_m \approx 21 \approx 3m^{-1}$. The size of our universe is only three times the Planck length. It is essential for our interpretation that as the lattices get bigger, the planckian regime shrinks in units of r_m . We found some evidence for this in our scaling analysis [5] where we ventured a scenario in which $\sqrt{G}/r_m \rightarrow 0$ because of triviality. This approach to zero might then be only logarithmic, which would make the problem of scale separation severe from the computational point of view. A careful study is needed to clarify these issues.

Acknowledgements

We thank Piotr Białas for useful discussions. The numerical simulations were carried out on the IBM SP1 at SARA and the Parsytec PowerXplorer at IC3A. This work is supported in part by FOM.

References

- [1] J. Ambjørn and J. Jurkiewicz, Phys. Lett. B278 (1992) 42.
- [2] M.E. Agishtein and A.A. Migdal, Mod. Phys. Lett. A7 (1992) 1039.
- [3] D. Weingarten, Nucl. Phys. B210 [FS6] (1982) 229.
- [4] G.W. Gibbons, S.W. Hawking and M.J. Perry, Nucl. Phys. B 138 (1978) 141.

- [5] B.V. de Bakker and J. Smit, Nucl. Phys. B 439 (1995) 239.
- [6] J. Ambjørn and J. Jurkiewicz, Nucl. Phys. B 451 (1995) 643.
- [7] P. Białas, Z. Burda, A. Krzywicki and B. Petersson, *Focusing on the fixed point of 4D simplicial gravity*, preprint LPTHE Orsay 96/08, BI-TP 96/05, ITFA-96-2, hep-lat/9601024.
- [8] B.V. de Bakker, *Further evidence that the transition of 4D dynamical triangulation is 1st order*, preprint AIAP-1996-040, hep-lat/9603024.
- [9] H.W. Hamber and R.M. Williams, Nucl. Phys. B 435 (1995) 361.
- [10] G. Modanese, Nucl. Phys. B 434 (1995) 697.
- [11] H.W. Hamber and S. Liu, Phys. Lett. B 357 (1995) 51.
- [12] B.V. de Bakker and J. Smit, Nucl. phys. (Proc. Suppl.) 34 (1994) 739.
- [13] B.V. de Bakker and J. Smit, *Correlations and binding in 4-d dynamical triangulation*, preprint ITFA-95-15, hep-lat/9510041.
- [14] S.R. Sharpe, in: *CP Violation and the limits of the Standard Model*, ed. J.F. Donoghue (World Scientific, 1995) p. 377.
- [15] J. Ambjørn, Z. Burda, J. Jurkiewicz and C.F. Kristjansen, Phys. Rev. D 48 (1993) 3695.
- [16] B.V. de Bakker and J. Smit, Nucl. Phys. B 454 (1995) 343.
- [17] P. Białas, private communication.
- [18] I. Antoniadis and E. Mottola, J. Math. Phys. 32 (1991) 1037.
- [19] M.E. Agishtein and A.A. Migdal, Nucl. Phys. B385 (1992) 395.
- [20] J. Ambjørn, J. Jurkiewicz and C.F. Kristjansen, Nucl. Phys. B393 (1993) 601.
- [21] B. Brüggmann, Phys. Rev. D 47 (1993) 3330.
- [22] S. Catterall, J. Kogut and R. Renken, Phys. Lett. B328 (1994) 277.
- [23] B.V. de Bakker and J. Smit, Phys. Lett. B 334 (1994) 304.

[24] R. Gupta, Nucl. Phys. B (Proc. Suppl.) 17 (1990) 70.